pISSN 2384-1095
eISSN 2384-1109

iMRI 2017;21:223-232

https://doi.org/10.13104/imri.2017.21.4.223

iMRI
Investigative Magnetic Resonance Imaging

Accelerated Resting-State Functional Magnetic Resonance Imaging Using Multiband Echo-Planar Imaging with Controlled Aliasing

Hyung Suk Seo[1*], Kyung Eun Jang[2*], Dingxin Wang[3,4], In Seong Kim[5], Yongmin Chang[6,7]

[1]Department of Radiology, Korea University Ansan Hospital, Gyeonggi-do, Korea
[2]Department of Medical & Biological Engineering, Kyungpook National University, Daegu, Korea
[3]MR R&D, Siemens Medical Solutions USA, Inc., Minneapolis, Minnesota, USA
[4]Radiology University of Minnesota, Minneapolis, Minnesota, USA
[5]Siemens Healthcare Ltd., Seoul, Korea
[6]Department of Radiology, Kyungpook National University Hospital, Daegu, Korea
[7]Department of Molecular Medicine, Kyungpook National University School of Medicine, Daegu, Korea

Original Article

Received: July 6, 2017
Revised: September 22, 2017
Accepted: October 7, 2017

*Both authors contributed equally to this work.

Correspondence to:
Yongmin Chang, Ph.D.
Department of Molecular Medicine & Radiology, Kyungpook National University School of Medicine, 200 Dongduk-ro, Jung-gu, Daegu 41944, Korea.
Tel. +82-53-420-5471
Fax. +82-53-422-2677
E-mail: ychang@knu.ac.kr

Purpose: To report the use of multiband accelerated echo-planar imaging (EPI) for resting-state functional MRI (rs-fMRI) to achieve rapid high temporal resolution at 3T compared to conventional EPI.

Materials and Methods: rs-fMRI data were acquired from 20 healthy right-handed volunteers by using three methods: conventional single-band gradient-echo EPI acquisition (Data 1), multiband gradient-echo EPI acquisition with 240 volumes (Data 2) and 480 volumes (Data 3). Temporal signal-to-noise ratio (tSNR) maps were obtained by dividing the mean of the time course of each voxel by its temporal standard deviation. The resting-state sensorimotor network (SMN) and default mode network (DMN) were estimated using independent component analysis (ICA) and a seed-based method. One-way analysis of variance (ANOVA) was performed between the tSNR map, SMN, and DMN from the three data sets for between-group analysis. $P < 0.05$ with a family-wise error (FWE) correction for multiple comparisons was considered statistically significant.

Results: One-way ANOVA and post-hoc two-sample t-tests showed that the tSNR was higher in Data 1 than Data 2 and 3 in white matter structures such as the striatum and medial and superior longitudinal fasciculus. One-way ANOVA revealed no differences in SMN or DMN across the three data sets.

Conclusion: Within the adapted metrics estimated under specific imaging conditions employed in this study, multiband accelerated EPI, which substantially reduced scan times, provides the same quality image of functional connectivity as rs-fMRI by using conventional EPI at 3T. Under employed imaging conditions, this technique shows strong potential for clinical acceptance and translation of rs-fMRI protocols with potential advantages in spatial and/or temporal resolution. However, further study is warranted to evaluate whether the current findings can be generalized in diverse settings.

Keywords: Multiband EPI; Resting-state fMRI; Resting-state network; Temporal SNR

INTRODUCTION

Multiband accelerated echo-planar imaging (EPI), in which multiple slices are excited and encoded simultaneously, enables major improvement in the spatial and/or temporal resolution of fMRI (1, 2). Higher temporal resolutions of multiband accelerated EPI has shown to improve overall statistical sensitivity and increase the content of information in the functional image (3). For example, it was demonstrated that multiband accelerated EPI was particularly advantageous for task-evoked high-resolution fMRI at an ultra-high field (1). More recently, multiband accelerated EPI has been used to improve data quality and increase the temporal sampling rate of resting-state fMRI (rs-fMRI) data to identify temporally independent modes that are robust and reproducible (3). rs-fMRI is emerging as an excellent tool for clinical studies because it does not impose attentional demands or cognitive burdens on the patient. Changes in functional connectivity in resting-state networks (RSNs) have been observed in a variety of diseases (4).

The higher temporal resolution of multiband accelerated EPI also provides a wider frequency spectrum of rs-fMRI data. By using a conventional gradient-echo EPI sequence, standard data acquisitions at 3T can achieve a temporal resolution of 2-3 s, which results in a maximum frequency of 0.3-0.5 Hz. In contrast, multiband accelerated EPI with a temporal resolution of 1 s results in a maximum frequency of 1 Hz. Spontaneous neural fluctuations in rs-fMRI data show that low-frequency fluctuations (less than 0.1 Hz) contribute to more than 90% of the correlation coefficient between regions of the same RSN (5, 6). However, as demonstrated in a previous study using conventional EPI sequence, aberrant high-frequency fluctuation (higher than 0.1 Hz) has been associated with a disease-related functional relevance in rs-fMRI data (7). Therefore, higher maximum frequency from multiband accelerated EPI may provide a wide frequency spectrum of rs-fMRI data to evaluate the aberrant high-frequency fluctuation higher than maximum frequency from conventional EPI sequence. Furthermore, higher sampling rates can be used with higher maximum frequency to reduce the temporal aliasing artifact of high-frequency noise sources and improve the characterization of the temporal and spatial features of RSNs (8, 9). Therefore, higher temporal resolution of multiband accelerated EPI can be used for either higher spatial resolution or shorter data acquisition time in rs-fMRI.

These findings suggest that multiband accelerated EPI has a significant advantage over conventional EPI for rs-fMRI data acquisition. However, the temporal signal-to-noise (tSNR) characteristics of multiband accelerated EPI time courses over tSNR characteristics of conventional EPI have not been fully investigated. Image time course stability has a critical importance in rs-fMRI data. Blood-oxygen level-dependent (BOLD) signal changes are often just a few tenths of a percent. Therefore, maximal sensitivity and high tSNR is required for reliable detection. Although several studies have examined the performance of a combined approach in which rs-fMRI data are acquired with a multiband and multi-echo acquisition (10, 11), the performance of multiband and single-echo EPI acquisition over conventional single-echo EPI acquisition in rs-fMRI has not been explored.

In this study, we report the use of multiband accelerated EPI for rs-fMRI to achieve rapid high-temporal resolution and whole-brain coverage at 3T. The signal-to-noise ratio (SNR), which reflects the static MRI signal-to-noise, does not provide insight into the temporal noise characteristics of fMRI time courses. Therefore, tSNR, which is calculated by dividing the mean of a time series by its standard deviation, was introduced to measure time course stability of rs-fMRI data using multiband accelerated EPI. tSNR of rs-fMRI data using conventional EPI was also measured for comparison. Finally, functional connectivity (FC) maps were evaluated using rs-fMRI data obtained from multiband accelerated EPI and conventional EPI, and statistical comparisons were made to evaluate the reliability of FC maps obtained from multiband accelerated EPI. Thus, our aim in this study was to evaluate tSNR of rs-fMRI data by using multiband accelerated EPI and to demonstrate that multiband accelerated EPI provides the same quality FC maps as rs-fMRI data using conventional EPI, suggesting that multiband accelerated EPI can provide potential advantages in the spatial and/or temporal resolution of rs-fMRI.

MATERIALS AND METHODS

Subjects

Twenty healthy right-handed volunteers (14 men and 6 women) between 23 and 36 years old (mean age, 28.6 years old) were recruited. Exclusion criteria included a history of brain injury, neurologic or psychiatric disease, or any major medical illness. Written informed consent was obtained from all participants. The study adhered to the Declaration of Helsinki and was approved by the Institutional Review Board of Korea University Hospital (IRB number: AS131454).

Functional Imaging Data Acquisition

rs-fMRI data were acquired at 3T using three different methods (Siemens Magnetom Skyra Syngo, Siemens Healthcare, Erlangen, Germany). First, conventional single-band gradient-echo EPI acquisition (Data set 1) was performed with the following sequence parameters: repetition time (TR)/echo time (TE) = 2000 ms/30 ms, flip angle = 90, field of view (FOV) = 210 mm, slice thickness = 4 mm, voxel size = 3.3 × 3.3 × 4 mm, number of slices = 37, total number of volumes = 240. Second, multiband gradient-echo EPI acquisition (Data set 2) was performed with the following sequence parameters: TR/TE = 1020 ms/30 ms, flip angle = 90, slice acceleration factor = 3, FOV = 190 mm, slice thickness = 3 mm, voxel size = 3.0 × 3.0 × 3.0 mm, number of slices = 51, total number of volumes = 480. Third, multiband gradient-echo EPI acquisition (Data set 3) was performed with the same sequence parameters as Data 2, except the total number of volumes was set to 240.

tSNR Analysis

Before tSNR analysis, all EPI images were processed using SPM8 (http://www.fil.ion.ucl.ac.uk/spm) with motion correction (i.e., realignment) for individual head movements, which was implemented in MATLAB (The MathWorks, Natick, MA, USA). tSNR maps were obtained per subject by dividing the mean of the time course of each voxel by its temporal standard deviation using processed EPI images. Specific mean tSNR maps of subjects were converted to Montreal Neurological Institute (MNI) space using previously calculated spatial normalization parameters and averaged across subjects. For within-group analysis, the group component was calculated as a random-effects map. SPM{t} was set to a threshold of $P < 0.05$, and a family-wise error (FWE) correction for multiple comparisons was applied across the whole brain. One-way repeated analysis of variance (ANOVA) was performed to compare differences across the three data sets. For direct comparisons, contrast images were assessed using a post-hoc t-test with Bonferroni correction, SPM{t} was set to a threshold of $P < 0.05$, and an FWE correction for multiple comparisons was applied at the voxel level. In addition, using the pre-processed EPI data (i.e., spatial normalization and averaged across subjects), the signal intensity of whole brain was plotted along with image volume.

Independent Component Analysis

Data analysis was performed using the SPM8 software package (http://www.fil.ion.ucl.ac.uk/spm) and Group independent component analysis (ICA) of the fMRI Toolbox software (GIFT, Version 1.3h; http://icatb.sourceforge.net/). Data preprocessing included realignment, spatial normalization, and Gaussian kernel smoothing with a full-width at half-maximum of 8 mm. Independent components (ICs) were identified in the low-frequency range (0.01-0.08 Hz) of the processed data. Data from all subjects were concatenated using the Infomax algorithm included in the software package. Total 184 ICs were calculated based on minimum description length (MDL) principle and were screened for the selection of the sensorimotor network (SMN) and default mode network (DMN). For within-group analysis, the group component was calculated as a random-effects map. The random-effects statistic for each voxel of the z-maps was generated using the ICA plug-in and calculated as the mean z-value of that voxel across the individual maps divided by its standard error, which resulted in a t-statistic. SPM{t} was set to a threshold of $P < 0.05$, and an FWE correction for multiple comparisons was applied across the whole brain. One-way repeated ANOVA was performed across the three data sets. For direct comparisons, SPM{t} was set to a threshold of $P < 0.05$, and an FWE correction for multiple comparisons was applied at the voxel level.

Seed-Based Analysis

The functional connectivity toolbox in SPM8 (http://web.mit.edu/swg/software.htm) was used to identify the resting-state SMN with a strong temporal correlation to a seed point in the right primary motor cortex. The M1 seed point in 5-mm radius spheres was identified using the MarsBar ROI tool (http://marsbar.sourceforge.net/) on MNI coordinates. In addition, the resting-state DMN was also identified with a 5-mm radius sphere seed point in the posterior cingulate cortex. Noise, cerebrospinal fluid, white matter, and motion parameters were used to correct time fluctuations of the BOLD signal as nuisance covariates, and a band-pass filter (0.01-0.08 Hz) was used. The results of individual functional connectivity maps were used for within-group analysis with SPM{t} set to a threshold of $P < 0.05$ (FWE-corrected for multiple comparisons at the voxel level) and a cluster size of 64 voxels. One-way repeated ANOVA was performed across the three data sets.

RESULTS

tSNR Study

Figure 1 shows the spatial normalization maps of tSNR

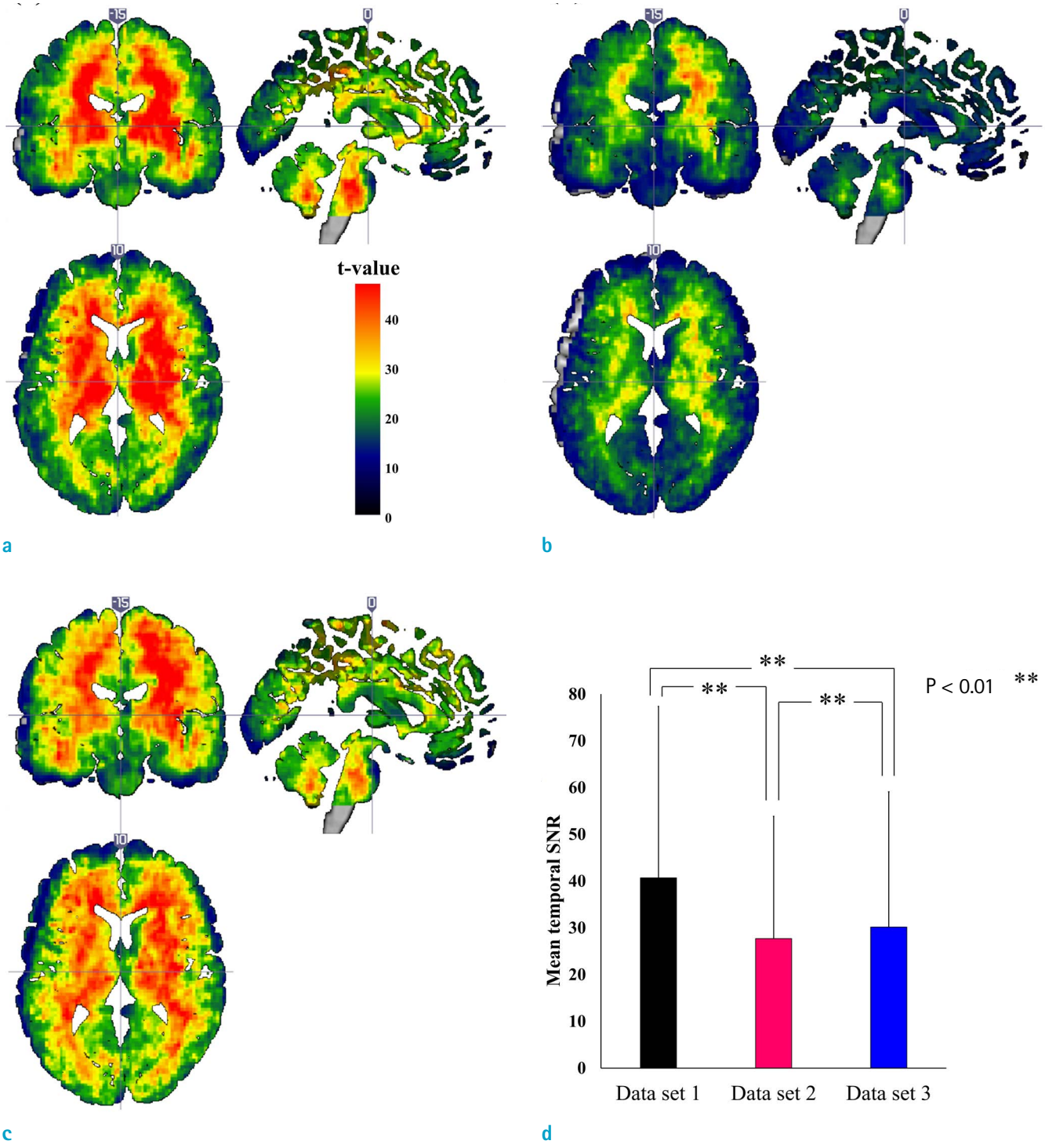

(a) Data set 1, (b) Data set 2, (c) Data set 3, (d) whole brain mean tSNR graph

Fig. 1. One sample t-test results from group maps of temporal signal-to-noise ratio (tSNR) for (a) Data set 1 (conventional echo-planar imaging [EPI]), (b) Data set 2 (multiband EPI with 480 volumes) and (c) Data set 3 (multiband EPI with 240 volumes). The SPM{t}s had a threshold of $P < 0.05$, with family-wise error (FWE)-correction for multiple comparisons at the whole brain level. Whole brain mean tSNR graphs were shown in (d).

for Data sets 1-3. These tSNR maps, which are averaged over subjects, show higher tSNR values in white matter than in gray matter, consistent with the pattern reported in the literature (12). The color gradient indicates the tSNR of the smoothed EPI time course data overlaid on the AFNI Talairach N27 atlas brain.

Results of the one-way ANOVA analysis showed tSNR differences in the striatum and medial and superior longitudinal fasciculus (Fig. 2a). Post-hoc two-sample t-tests showed tSNR was higher in Data set 1 than in Data sets 2 and 3 in these brain regions (Fig. 2b, c).

ICA-Based Analysis

Figure 3a and b compare three SMN components and

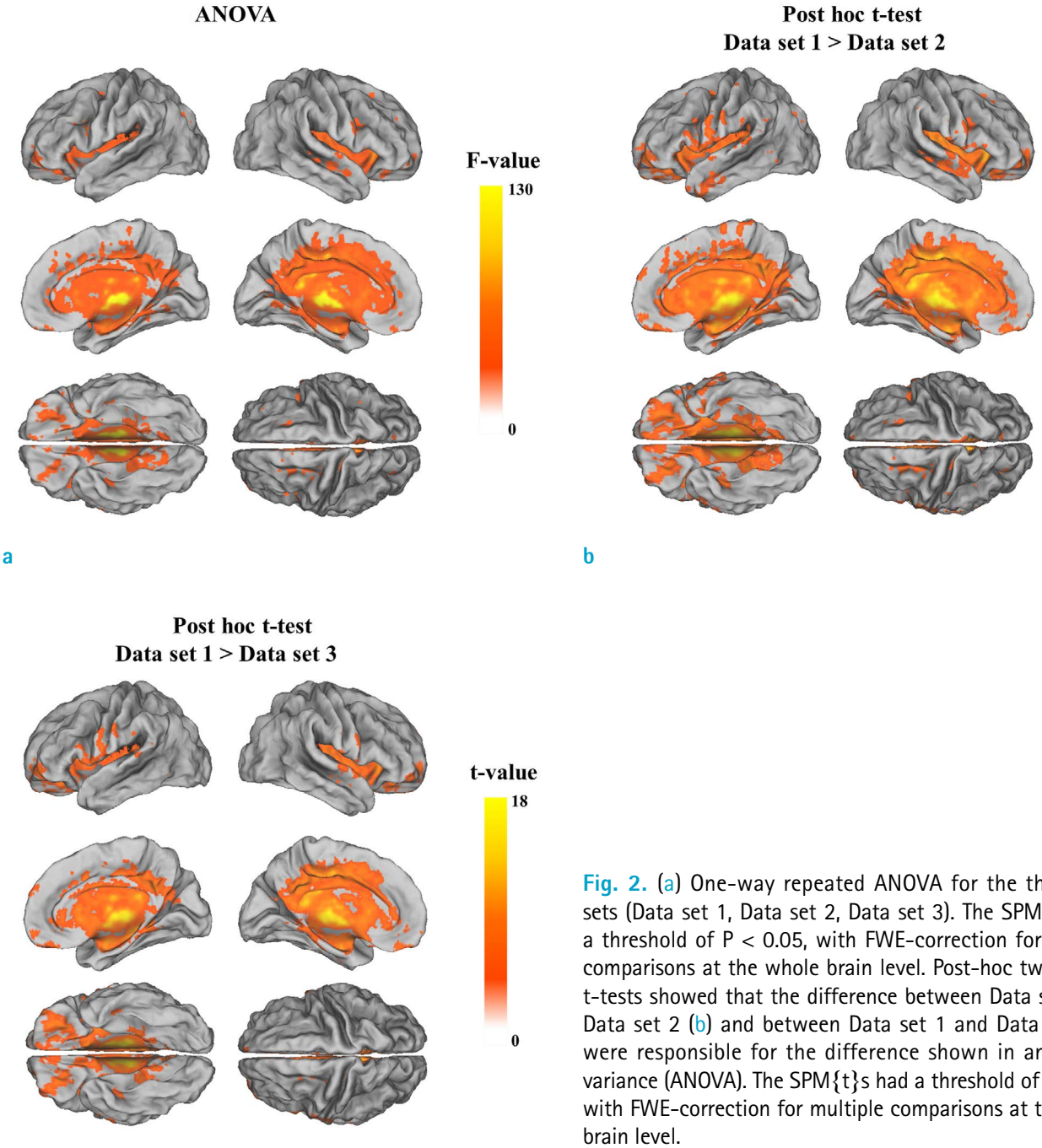

Fig. 2. (a) One-way repeated ANOVA for the three data sets (Data set 1, Data set 2, Data set 3). The SPM{F}s had a threshold of $P < 0.05$, with FWE-correction for multiple comparisons at the whole brain level. Post-hoc two sample t-tests showed that the difference between Data set 1 and Data set 2 (b) and between Data set 1 and Data set 3 (c) were responsible for the difference shown in analysis of variance (ANOVA). The SPM{t}s had a threshold of $P < 0.05$, with FWE-correction for multiple comparisons at the whole brain level.

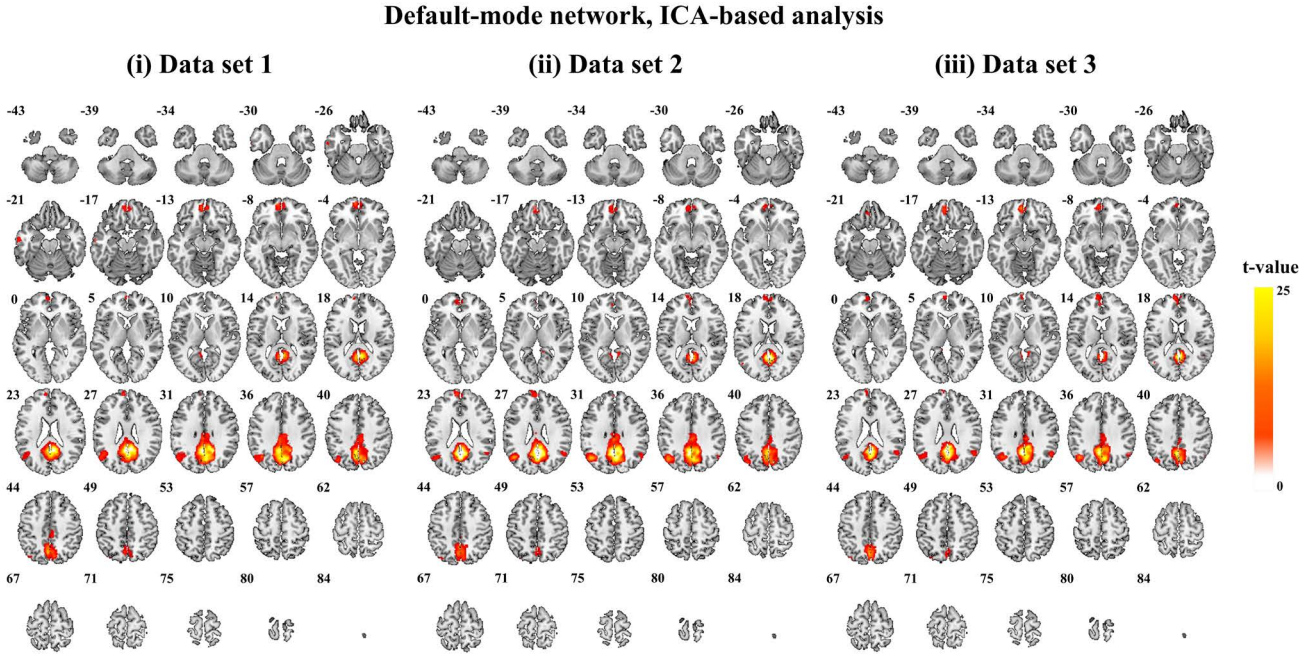

a

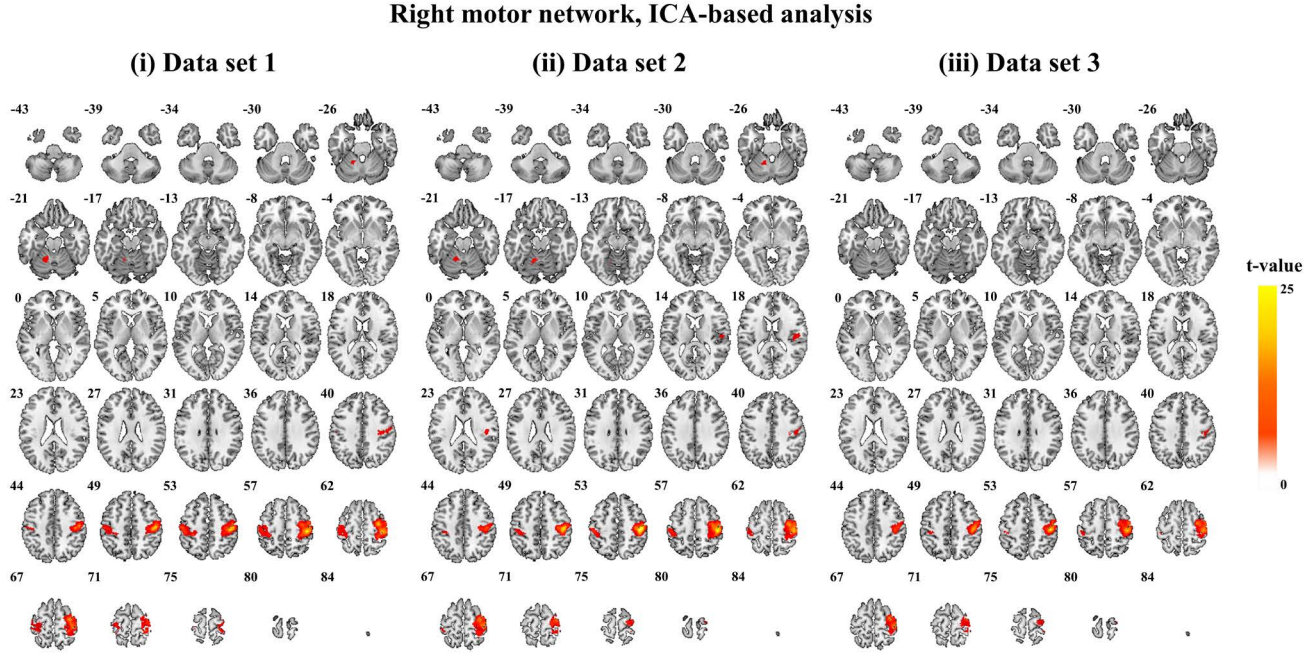

b

Fig. 3. One sample t-test results of (a) default-mode networks and (b) right motor networks obtained from independent component analysis for three data sets (Data set 1, Data set 2, Data set 3). The SPM{t}s had a threshold of $P < 0.05$, with FWE-correction for multiple comparisons at the whole brain level. One-way repeated ANOVA for the three data sets did not show differences between data sets.

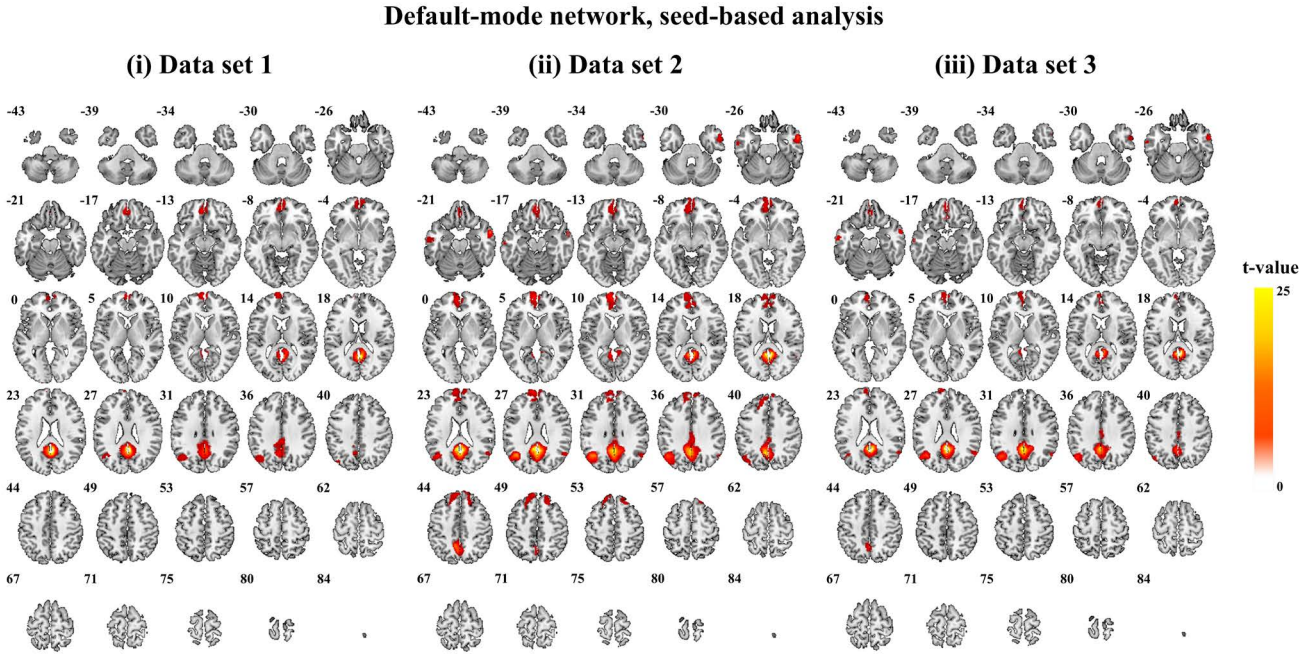

a

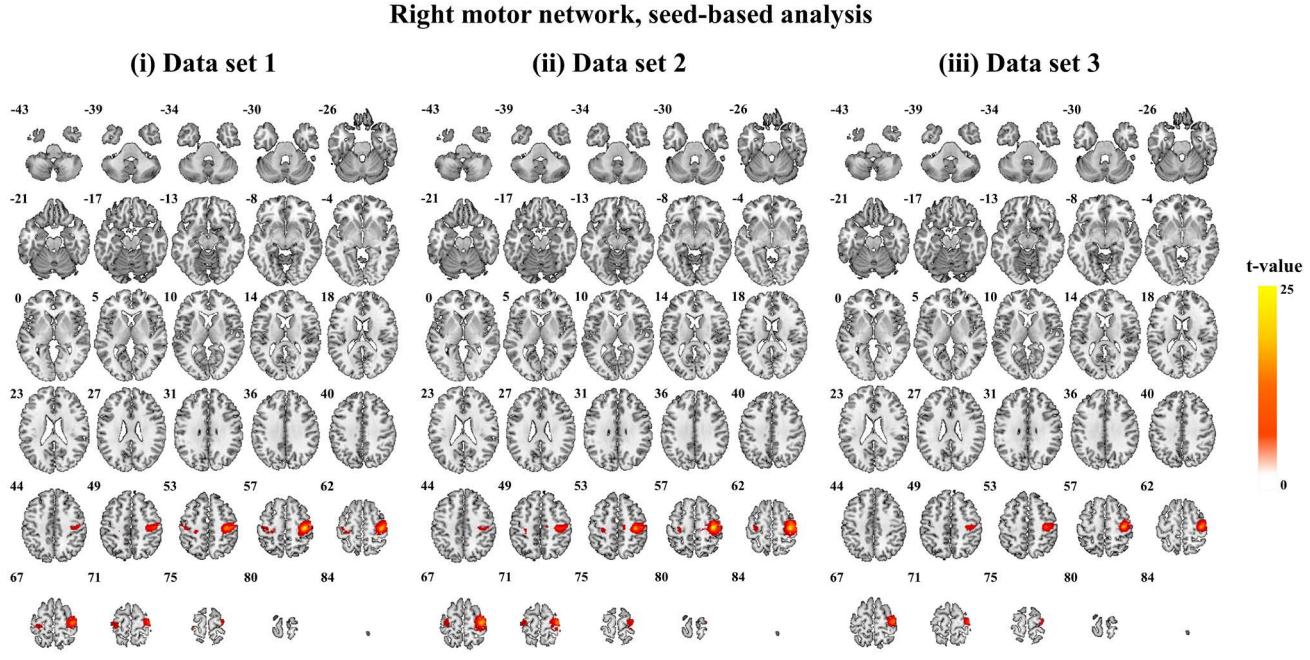

b

Fig. 4. One sample t-test results of (a) default-mode networks and (b) right motor networks obtained from seed-based analysis for three data sets (Data set 1, Data set 2, Data set 3). The SPM{t}s had a threshold of $P < 0.05$, with FWE-correction for multiple comparisons at the whole brain level. One-way repeated ANOVA for the three data sets did not show differences between data sets.

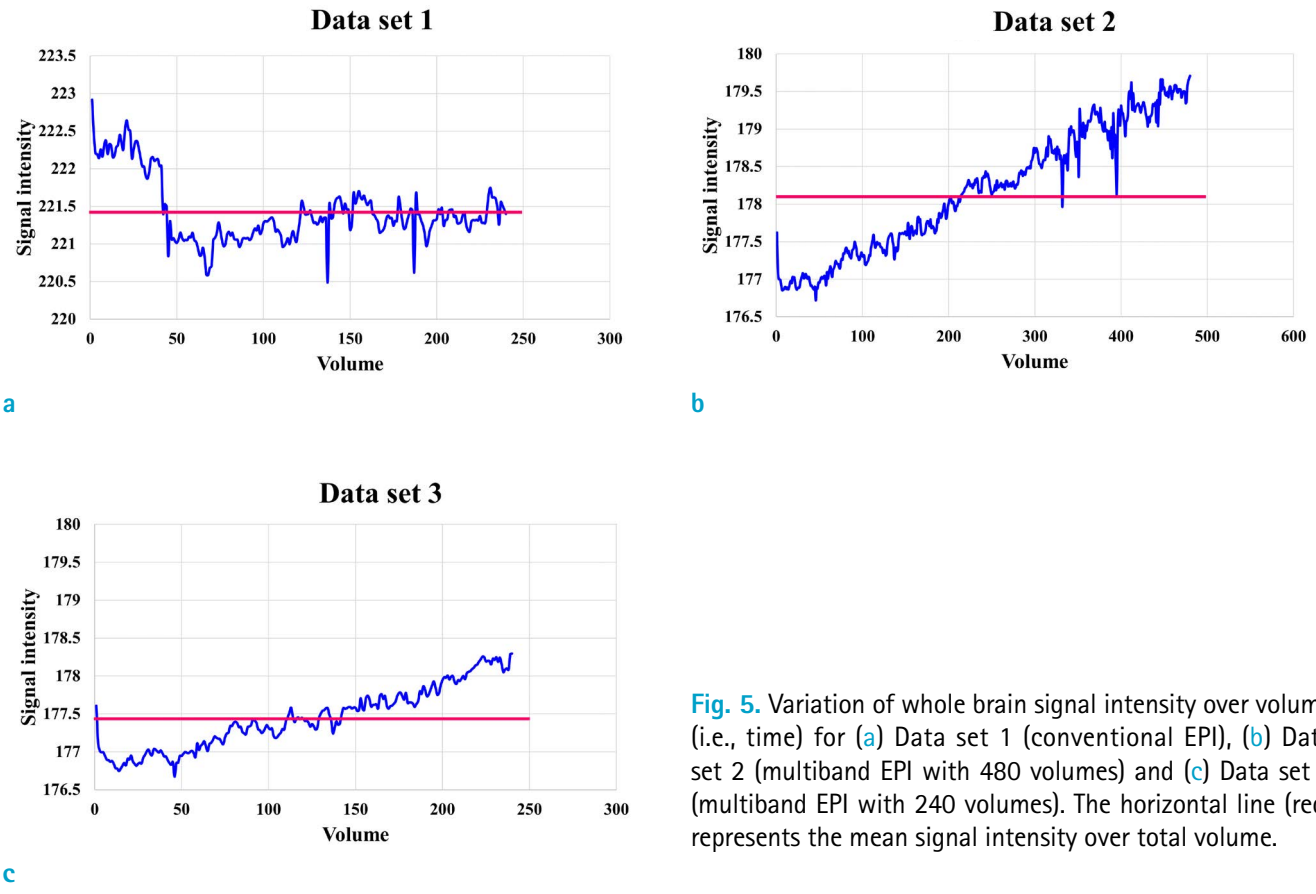

Fig. 5. Variation of whole brain signal intensity over volume (i.e., time) for (a) Data set 1 (conventional EPI), (b) Data set 2 (multiband EPI with 480 volumes) and (c) Data set 3 (multiband EPI with 240 volumes). The horizontal line (red) represents the mean signal intensity over total volume.

three DMN components, respectively, derived from spatial ICA decompositions of the three resting-state group data sets. One-way ANOVA revealed no significant differences between the three SMN and three DMN components.

Seed-Based Analysis

Figure 4a and b compare three SMN components, derived from a seed in the left sensorimotor cortex, and three DMN components, from a seed in the posterior cingulate cortex, respectively, in the three resting-state group data sets. One-way ANOVA revealed no significant differences between the three SMN and three DMN components.

DISCUSSION

In this study, rs-fMRI results except tSNR were similar between multiband accelerated EPI data and conventional EPI data within the adapted metrics estimated under specific imaging conditions employed in this study. This study therefore shows that the introduction of multiband imaging reduces TR and does not cause any adverse effects at 3T. That is, by maintaining the image quality comparable to that of conventional EPI, multiband accelerated EPI with short TR can acquire the same volume of rs-fMRI data much faster than conventional EPI.

ANOVA analysis of FC maps obtained from both ICA and a seed-based method showed that there was no difference in the resting-state networks (i.e., SMN and DMN) among the three different data sets with the adapted metrics estimated under employed imaging conditions in this study. These results therefore suggest that multiband accelerated EPI can provide BOLD EPI data for an rs-fMRI study with a much shorter acquisition time or can provide more data volumes in the same acquisition time than conventional EPI. Recent studies have demonstrated that the total volume can be increased using multiband accelerated EPI with short TR (13, 14). High rs-fMRI data volume and high frequency with short TR are important for tracking dynamic resting-state networks at higher frequencies (12). Dynamic fluctuations in the functional connectivity of resting-state networks at higher frequencies might represent a balance

between optimizing information processing and minimizing metabolic expenditure (14).

In all three data sets, tSNR was higher in white matter than in gray matter, which is consistent with the findings of previous reports (11). Our ANOVA analysis revealed that tSNR was higher in conventional EPI than in multiband accelerated EPI, mostly in white matter structures. Furthermore, multiband EPI with 480 volumes showed lower tSNR compared to multiband EPI with 240 volumes primarily because multiband EPI with 480 volumes has large variation in signal intensity over volumes (i.e., time) and thus has large temporal standard deviation (Fig. 5). Therefore, it is interesting to know how tensor metrics, such as fractional anisotropy maps and fiber tractography, from diffusion tensor imaging are influenced when using multiband accelerated EPI than those using conventional EPI. Furthermore, it should be noted that while optimal setting of flip angle is important for tSNR evaluation, the flip angle (90 degree) used for both conventional EPI and multiband EPI is somewhat suboptimal for white and gray matter on 3T with experimental condition in the current study. Therefore, further work is needed to explore the relative sensitivity of multiband accelerated EPI to tSNR measurement and diffusion tensor imaging.

One inherent concern with multiband imaging and rs-fMRI is the leakage of RSNs onto other aliased slices due to multi-slice acquisition (15). Recently, ICA-based X-noiseifier, which is an ICA-based correction, has been proposed as a method to detect and remove these leakage artifacts due to multi-slice acquisition (9). Another concern is that spurious correlations due to suboptimal image reconstruction may be interpreted as real RSNs (16).

In conclusion, under specific employed imaging conditions, the multiband accelerated EPI pulse sequence significantly increased the temporal resolution of whole-brain rs-fMRI and substantially reduced scan times at 3T. It was also shown that multiband accelerated EPI provides the same quality FC maps as conventional EPI within the adapted metrics estimated under specific imaging conditions employed in this study. This technique can be used to expand and enrich functional information obtained from rs-MRI with high maximum frequency if the findings can be hold true for more general settings. Furthermore, reduced scan times may facilitate the clinical acceptance and translation of rs-fMRI protocols. However, it should be noted that depending on the objective of a study, it is the recording time of spontaneous activity, rather than the brevity of scanning time, that matters in clinical investigations. Therefore, it is necessary to investigate further to evaluate whether the present findings under specific settings can be generalized in more diverse settings.

Conflict of Interest Statement

The authors declare that there are no conflicts of interest.

Acknowledgments

This work was supported by National Research Foundation of Korea (NRF) funded by the Ministry of Science (2013R1A1A1012361).

REFERENCES

1. Moeller S, Yacoub E, Olman CA, et al. Multiband multislice GE-EPI at 7 tesla, with 16-fold acceleration using partial parallel imaging with application to high spatial and temporal whole-brain fMRI. Magn Reson Med 2010;63:1144-1153
2. Setsompop K, Gagoski BA, Polimeni JR, Witzel T, Wedeen VJ, Wald LL. Blipped-controlled aliasing in parallel imaging for simultaneous multislice echo planar imaging with reduced g-factor penalty. Magn Reson Med 2012;67:1210-1224
3. Smith SM, Miller KL, Moeller S, et al. Temporally-independent functional modes of spontaneous brain activity. Proc Natl Acad Sci U S A 2012;109:3131-3136
4. Cole DM, Smith SM, Beckmann CF. Advances and pitfalls in the analysis and interpretation of resting-state FMRI data. Front Syst Neurosci 2010;4:8
5. Cordes D, Haughton VM, Arfanakis K, et al. Frequencies contributing to functional connectivity in the cerebral cortex in "resting-state" data. AJNR Am J Neuroradiol 2001;22:1326-1333
6. Leopold DA, Murayama Y, Logothetis NK. Very slow activity fluctuations in monkey visual cortex: implications for functional brain imaging. Cereb Cortex 2003;13:422-433
7. Malinen S, Vartiainen N, Hlushchuk Y, et al. Aberrant temporal and spatial brain activity during rest in patients with chronic pain. Proc Natl Acad Sci U S A 2010;107:6493-6497
8. Feinberg DA, Moeller S, Smith SM, et al. Multiplexed echo planar imaging for sub-second whole brain FMRI and fast diffusion imaging. PLoS One 2010;5:e15710
9. Griffanti L, Salimi-Khorshidi G, Beckmann CF, et al. ICA-based artefact removal and accelerated fMRI acquisition for improved resting state network imaging. Neuroimage 2014;95:232-247
10. Olafsson V, Kundu P, Wong EC, Bandettini PA, Liu TT. Enhanced identification of BOLD-like components with

multi-echo simultaneous multi-slice (MESMS) fMRI and multi-echo ICA. Neuroimage 2015;112:43-51
11. Boyacioglu R, Schulz J, Koopmans PJ, Barth M, Norris DG. Improved sensitivity and specificity for resting state and task fMRI with multiband multi-echo EPI compared to multi-echo EPI at 7 T. Neuroimage 2015;119:352-361
12. Hutton C, Josephs O, Stadler J, et al. The impact of physiological noise correction on fMRI at 7 T. Neuroimage 2011;57:101-112
13. Lee HL, Zahneisen B, Hugger T, LeVan P, Hennig J. Tracking dynamic resting-state networks at higher frequencies using MR-encephalography. Neuroimage 2013;65:216-222
14. Zalesky A, Fornito A, Cocchi L, Gollo LL, Breakspear M. Time-resolved resting-state brain networks. Proc Natl Acad Sci U S A 2014;111:10341-10346
15. Moeller S, Xu J, Auerbach EJ, Yacoub E, Ugurbil K. Signal leakage (L-factor) as a measure for parallel imaging performance among simultaneously multi-slice (SMS) excited and acquired signals. In Proceedings of the 20th Annual Meeting of ISMRM, Melbourne, Australia, 2012. Abstract 519
16. Setsompop K, Polimeni JR, Bhat H, Wald LL. Characterization of artifactual correlation in highly-accelerated simultaneous multi-slice (SMS) fMRI acquisitions. In Proceedings of the 21th Annual Meeting of ISMRM, Salt Lake City, Utah, USA, 2013. Abstract 410